Chapter-4

Study of Phase Transition & its Effects on Current Voltage Hysteresis in novel Copper Tin(II) Iodide

Phase Transition Eeffcts on Current Voltage Hysteresis in novel $CuSnI_3$.

Prem C. Bharti, S. Singh, Pardeep K. Jha, Priyanka A. Jha and Prabhakar Singh.(under preparation)

CHAPTER 4: Study of Phase Transition & its Effects on Current Voltage Hysteresis in novel Copper Tin(II) Iodide

4.1 Introduction

Perovskite halides are known to undergo various phase transitions, such as transitions between deferent crystal structures as a function of temperature [218], pressure [219], or compositional changes [220]. These transitions can lead to substantial changes in the material's band structure [221], carrier mobility [222], and defect density [223], all of which play crucial roles in the photoelectric behaviour [224]. For instance, a phase transition may lead to the formation or annihilation of defect states [225] that act as traps for charge carriers [226], thus affecting the recombination dynamics [227] and the overall photo response [228]. Similarly, changes in the crystal structure can influence ion migration pathways [229], which are closely linked to hysteresis effects. The alignment and movement of ions such as halides and organic cations within the perovskite lattice can be significantly altered during phase transitions, impacting the stability and reproducibility of the photoelectric response.

Here, we are studying lesser known [230] $CuSnI_3$ in order to explore the photo hysteresis behaviour in non-centrosymmetric phase. Understanding how phase transitions affect photoelectric hysteresis in perovskite halides is essential for improving the performance and durability of perovskite based devices. By elucidating the mechanisms through which phase transitions influence hysteresis, researchers can develop strategies to control and mitigate these effects, leading to more stable and efficient devices. This knowledge is particularly important

for the development of next-generation solar cells, to counter hysteresis problem which can lead to performance instability and degradation over time.

4.2 Experimental Details

The powder sample of $CuSnI_3$ was prepared by cold-sintering (solid state reaction) technique at room temperature. The precursor SnI_2 and CuI (M/s Alfa Aesar, 99.9%) were mixed in stoichiometric ratios and ground in mortar pestle for 2 hours in ambient environment and ice bath and finally we get pale yellow-brown colour powder of $CuSnI_3$. Further, powder was pelletized using hydraulic press at a pressure of 5 tons and sintered at 5 ℃ in ice bath at refrigerator [207]. The X-ray diffraction (XRD) of the pellet samples was performed in the range of $2\theta = 5° - 120°$ at the step of 2°/min. The band gap was analysed using optical absorption spectrum and the I-V measurement was obtained in dark and on the exposure to the radiation through Science tech solar simulator class: AAA with AM 1.5 G. Further, the impedance measurement of the studied samples is done before and after exposure of light using Solartron 1260 A impedance analyser at different oscillation amplitudes ranging from 0.125 V to 1 V at the steps of 0.125 V. The high temperature Raman spectroscopic studies were carried out in a backscattering configuration using a LabRam HR evo system equipped with a liquid helium cryogenic facility. An Ar^+ laser of 633 nm as excitation source, 1800 g/mm grating, and a charge coupled device (CCD) detector was used for the measurements.

4.3 Results and Discussion

4.3.1 Structural Prediction, Phase Transition and Hysteresis

$CuSnI_3$ is a lesser-known compound and is only predicted to have a hexagonal structure. In the present work, the structure of $CuSnI_3$ is predicted using the trial and error method. It is crystallized in the three-dimensional Spinnel structured triclinic P3m1 space group at 300 K. Cu^{2+} is bonded to four I^- atoms to form CuI_4 tetrahedra that share corners with twelve SnI_6 octahedra. The corner-sharing octahedra tilt angles range from 58-59°. There are three shorter (2.00 Å) and one longer (2.01 Å) Sn-I bond lengths. There are four inequivalent Sn^{4+} sites. In the first Sn^{4+} site, Sn^{4+} is bonded to six I^- atoms to form SnI_6 octahedra that share corners with six equivalent CuI_4 tetrahedra and edges with six SnI_6 octahedra. Four shorter (2.06 Å) and two longer (2.07 Å) Sn-I bond lengths exist. In the second Sn^{4+} site, Sn^{4+} is bonded to six I^- atoms to form SnI_6 octahedra that share corners with six equivalent CuI_4 tetrahedra and edges with six SnI_6 octahedra. There is a spread of Sn-I bond distances ranging from 2.05-2.07 Å. In the third Sn^{4+} site, Sn^{4+} is bonded to six I^- atoms to form SnI_6 octahedra that share corners with six equivalent CuI_4 tetrahedra and edges with six SnI_6 octahedra. There are four shorter (2.06 Å) and two longer (2.07 Å) Sn-I bond lengths. In the fourth Sn^{4+} site, Sn^{4+} is bonded to six I^- atoms to form SnI_6 octahedra that share corners with six equivalent CuI_4 tetrahedra and edges with six SnI_6 octahedra. There are four shorter (2.06 Å) and two longer (2.07 Å) Sn-I bond lengths. There are four inequivalent I^- sites. In the first I^- site, I^- is bonded to one Cu^{2+} and three Sn^{4+} atoms to form a mixture of distorted edge and corner-sharing CuSnI3trigonal pyramids. In the second I site, I^- is bonded to one Cu^{2+} and three Sn^{4+} atoms to form a mixture of distorted edge and corner-sharing $CuSnI_3$ trigonal pyramids. In the third I^- site, I^- is bonded

to one Cu^{2+} and three Sn^{4+} atoms to form a mixture of distorted edge and corner-sharing $CuSnI_3$ trigonal pyramids. In the fourth I^- site, I^- is bonded to one Cu^{2+} and three Sn^{4+} atoms to form a mixture of distorted edge and corner-sharing $CuSnI_3$ trigonal pyramids.

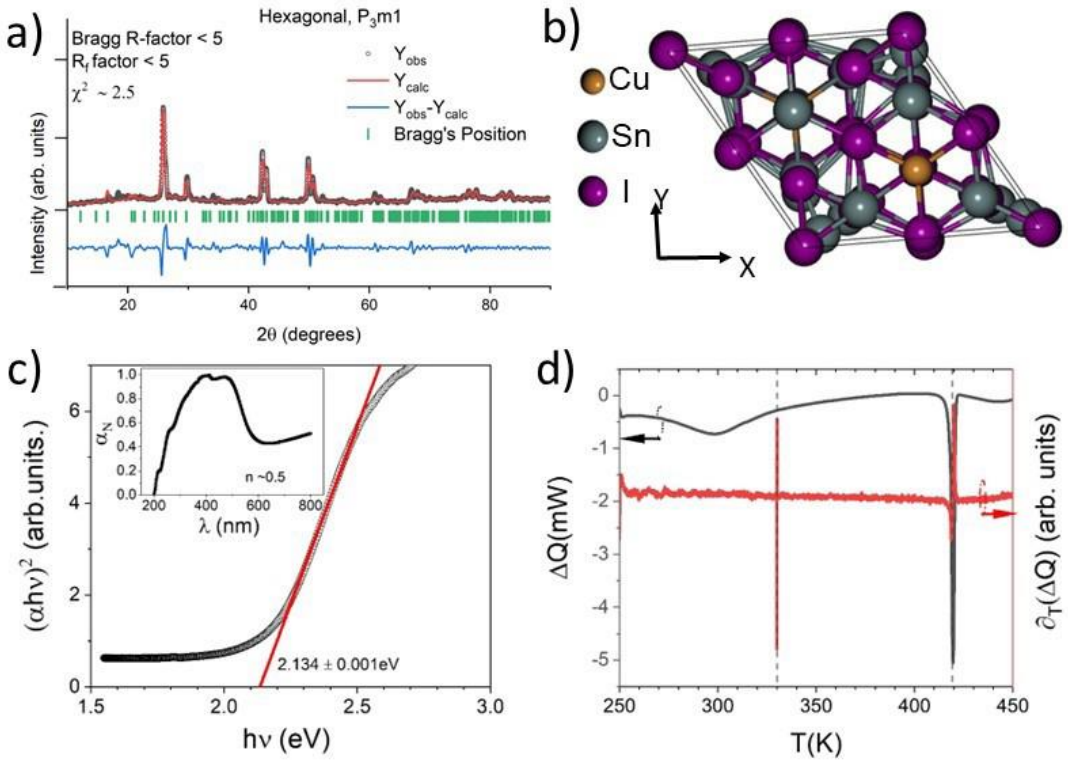

Figure 4.1 a) XRD b) crystal structure, c) band gap estimation from Tauc plots (inset) UV absorbance curve with wavelength, d) DSC curves.

The band gap ~2.13eV is estimated using Tauc plots[199][201][207][231] (Figure 4.1c). The nature of bandgap is direct as transmission mode, n = 0.5 (Figure 4.1c inset). To understand the formation mechanism of $CuSnI_3$, heat variation ΔQ is plotted with temperature, T. It can be seen that there is a heat loss below 300 K suggesting its formation between 250 K and 300 K. In addition, an endothermic peak is formed at 423 K. The endothermic peaks are verified with the derivative and discontinuities are observed at 323 K (T_I) and 423 K (T_{II}). These

discontinuities appear due to phase transitions. Thus, these anomalies are further inspected using conductivity measurements with temperature.

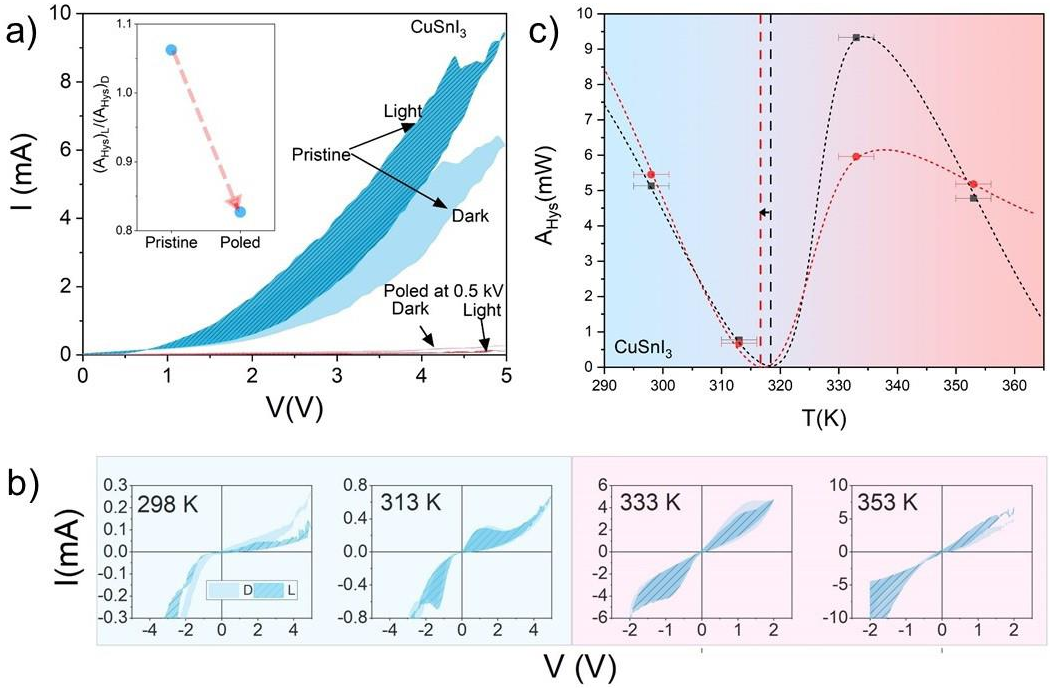

Figure 4.2 a) I-V Curve for Pristine and Poled sample in dark and light (AM 1.5 G) condition at 300 K (inset) suggest in Poled sample hysteresis area (A_{Hys}) reduced in light while in case of Pristine sample, A_{Hys} is greater as compare to dark. b) I-V Curve for Pristine and Poled sample in dark and light at 298 K, 313 K, 333 K and 353 K c) variation of A_{Hys} with temperature in dark and light conditions

In order to explore the influence these possible phase transition on current voltage hysteresis here we studied the temperature dependent behaviour of current voltage curve both in dark and light i.e., AM 1.5 G around the possible anomalies/phase transitions [202]. In order to get intrinsic behaviour around these anomalies, we have poled the sample at electric field 0.5 kV for 30 minutes and compared the current voltage behaviour with pristine sample (Figure 4.2a) at 300 K in ambient conditions. A significant decrease in current is observed in poled sample (typically in light) and therefore current voltage hysteresis (Figure 4.2a (inset)). The volatile nature of these Perovskite halides at higher temperature (> 400 K), typically in the presence of

light, restricted our study in temperature range of 298 K-353 K only (Figure 4.2b). We observe sudden increase in current value for $T > T_I$. Then, we estimated hysteresis area (A_{Hys}) for IV curves and found that there is a sharp reduction in the A_{Hys} ($\rightarrow 0$) in the vicinity of T_I (Figure 4.2c). Significantly, in the presence of light, the hysteresis area does not alter around T_I.

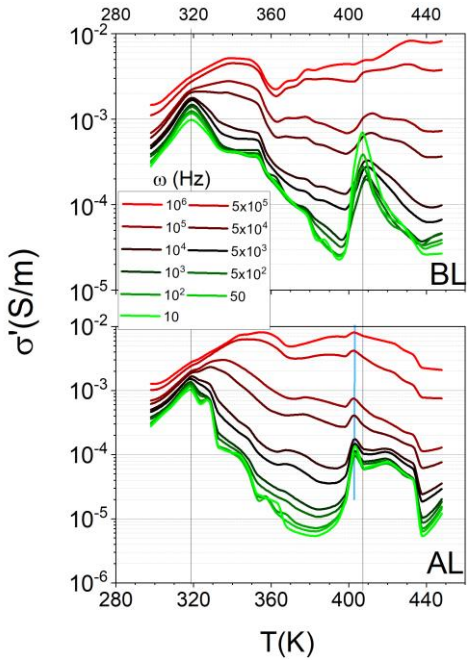

Figure 4.3 Temperature dependent conductivity measurements at different frequencies.

The sample degraded after 400 K, in order to inspect the degradation behaviour with temperature, ac conductivity is plotted before and after light exposure(Figure 4.3). It can be seen that in the pristine sample, two sharp phase transitions are appearing at ~319 K (I) and ~408 K (II). However, some anomalies are observed in between 360 K and 408 K. After light exposure, the transition temperature of sharp phase transition (II) has reduced to 402 K. However, the nature of phase transitions has not changed after light exposure and the anomalies observed in between 360 K and 408 K have become more prominent after light exposure.

4.3.2 Ionic Conduction behaviour at phase transition

Reduction in the hysteresis area, at phase transition T_I, can enliht the cause of hysteresis. In halides, ion conduction is well known, while phase transition usually links to parameter related to electronic contribution. The conductivity is due to either due to band conduction and hopping of ions in localised states. Thus, to study the ion movement around the transitions, ac conductivity isotherms are fitted with Jonscher power law [232]; $\sigma = \sigma_{dc}(1 + (\omega/\omega_H)^s)$.

The variation of parameters dc conductivity (σ_{dc}), hopping frequency (ω_H) and frequency exponent (s) are extracted and variation of these parameters with temperature are plotted respectively (Figure 4.4a-c). The change in features is observed along each transition. There is maxima at ~320 K followed by a maxima at ~408 K in the dc conductivity curve (Figure 4a) in the pristine sample as well as sample after light exposure. It is also seen that there is a minima at ~320 K in the exponent curve and is observed to further increase with the increase in temperature in the pristine sample as well as sample after light exposure.

Whereas, in the hopping frequency curve, a plateau is observed starting at ~320 K and ending at ~408 K in the pristine sample whereas a delta is formed starting at ~320 K and ending at ~408 K in the sample after light exposure.

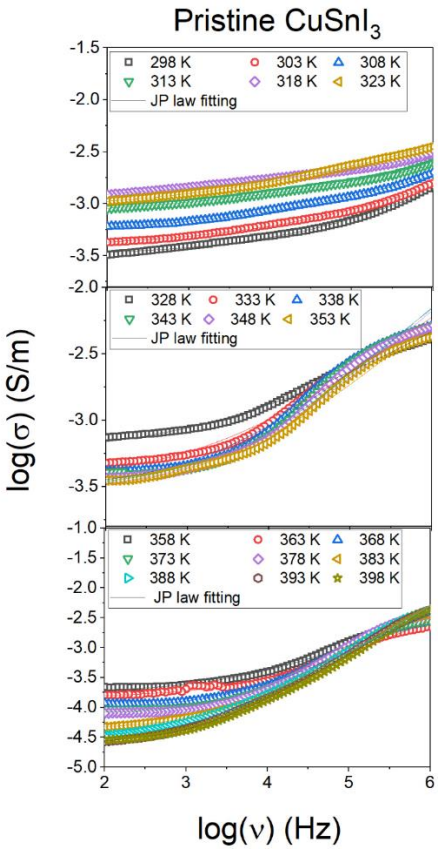

Figure 4.4 J-P law fitting in pristine $CuSnI_3$.

4.3.3 Vibrational mode behaviour at phase transition

As revealed from Rietveld refinement of XRD data, the refinement has been achieved with $P3m1$ symmetry. In crystallography, space group $P3m1$ indicates a threefold rotational symmetry with a mirror plane perpendicular to the rotation axis. This affects the selection rules for Raman scattering. The point group of the space group $P3m1$ is $C3v$ (3m) and has a threefold rotational axis and three vertical mirror planes. For C3v, the irreducible representations are $A1$, $A2$ and $E, A1$ is symmetric with respect to the principal axis and mirrors. $A2$ is antisymmetric with respect to the mirrors and E are doubly degenerate modes (in-plane vibrations). However, for $C3v$ symmetry, $A1$ and E are Raman active modes that

involve symmetric stretching or compressing along the principal axis and in-plane vibrations, respectively. We have observed E modes at positions $\omega 1, \omega 4$ and $\omega 5$ while A-modes are observed at ω2, ω3 (Fig.4.5 and 4.6a). With the increase in temperature at 325 K, the normalised intensity for E-mode at $\omega 1$ increases while the normalised intensity for A-mode at $\omega 2$ decreases (Figure 4.6 b). A broad peak with two doublets is observed at 250K, this doublet has formed a new peak at $\omega 1$ and a single sharp peak remains at $\omega 2$. However, at 325K, three features are visible i.e. a new peak at $\omega 1$ along with a doublet at $\omega 2$.

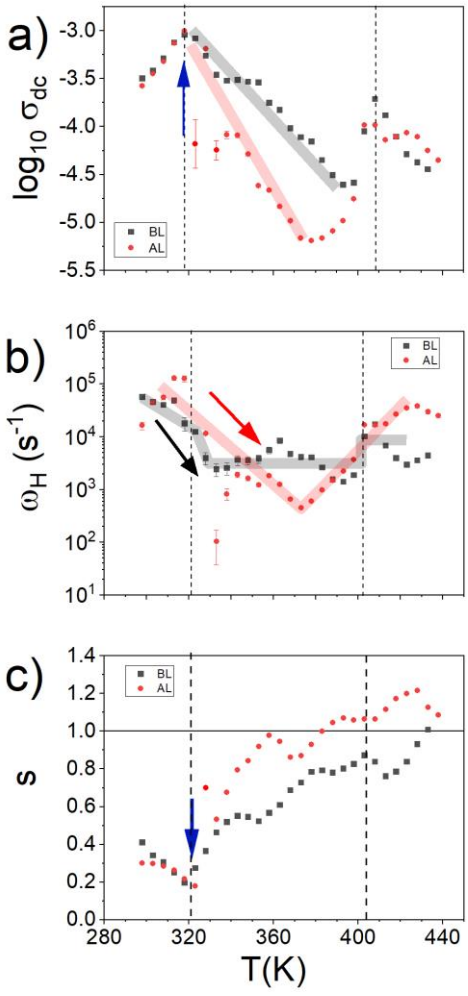

Figure 4.5 The variation of parameters a) dc conductivity($\boldsymbol{\sigma_{dc}}$), b) hopping frequency (ω_H) and c) frequency exponent (s) with temperature

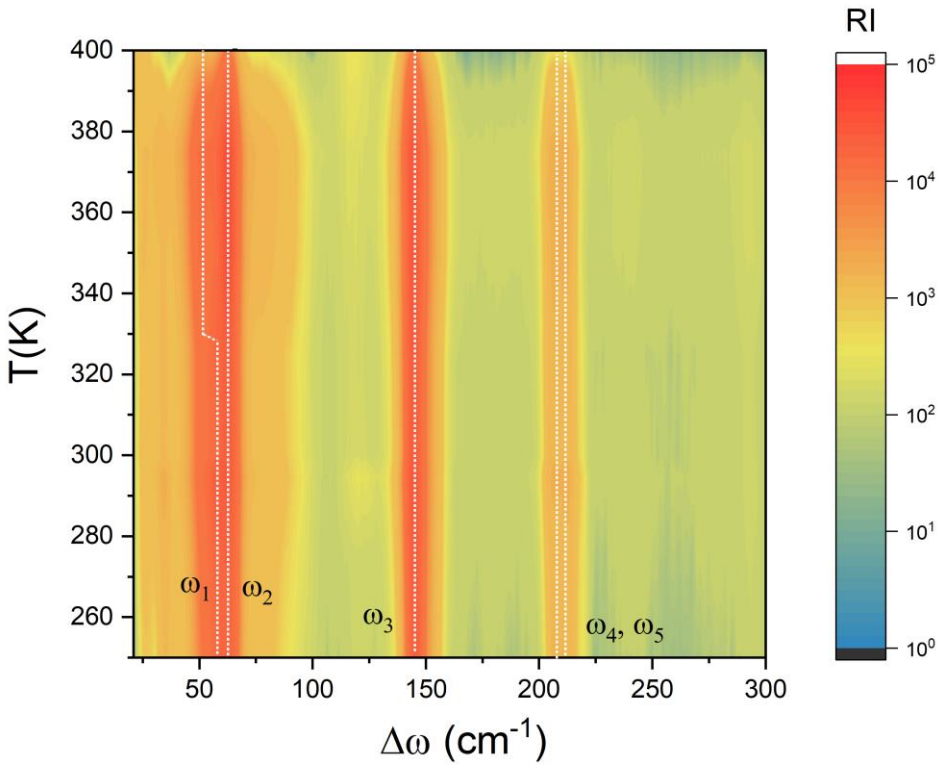

Figure 4.6 High temperature Raman spectra of $CuSnI_3$

According to Group-Subgroup theory, the possible super group of $P3m1$ are $Pm31$ and/or $R3m$ and ultimate to cubic phase [233]. Thus, at 325 K, $P3m1$ transforms to R3m and R3m further transforms to cubic phase at 425 K.

The E mode corresponds to the free SnI_4 molecule and with the changes in crystal environment, molecule equilibrium changes as compared to the free state. A small SnI_4 tetrahedron distortion has led to the splitting of E symmetry vibration modes with temperature. However, the static field effects in SnI are connected with the position symmetry of SnI molecules in the lattice.

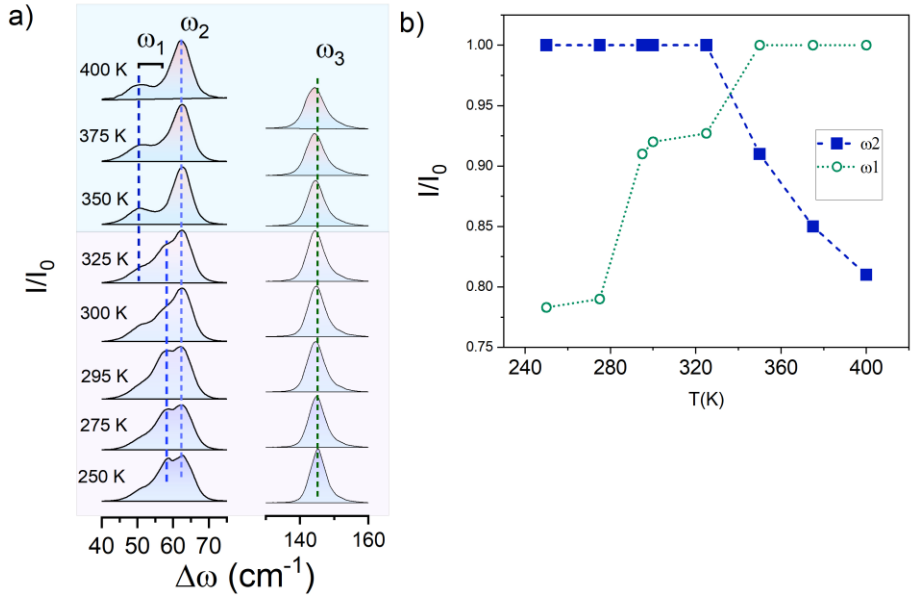

Figure 4.7 Variation of a) normalised intensity with wave number for A and E modes at different temperatures b) mode corresponding tp Raman shift ω_1 and ω_2 with temperature.

Thus, the normal vibration can be seen as linear combinations of SnI molecule displacements with their orientation conditioned by weak resonant Van der Waals intramolecular interactions. Furthermore, Raman intensity of E-mode increases at isomorphic phase transition and therefore polarizability, especially electronic polarizability α_e (coupled with $\triangle Pe$) should increase at 325 K.

4.4 Conclusion

Our study on $CuSnI_3$ reveals significant insights into the impact of phase transitions on photoelectric hysteresis in perovskite halides. $CuSnI_3$ exhibits a triclinic $P3m1$ structure at 300 K, with phase transitions observed at ~320 K and ~408 K. These transitions influence the material's electronic properties, defect states, and ion migration pathways, affecting its photoelectric response. I-V measurements indicate a sharp reduction in hysteresis area around

the first phase transition, highlighting the critical role of phase transitions in modulating hysteresis behaviour. AC conductivity studies further corroborate these findings, showing distinct changes in dc conductivity, hopping frequency, and frequency exponent across the phase transitions. Raman spectroscopy supports the structural changes observed, with shifts in E and A modes indicating symmetry changes and molecular distortions. This comprehensive understanding of phase transition effects on photoelectric hysteresis can guide the development of more stable and efficient perovskite-based devices, addressing performance instability and degradation challenges.